applied sciences

MDPI

Article

Recovery and Characterization of Orbital Angular Momentum Modes with Ghost Diffraction Holography

Yanyan Huang [1], Vinu R.V. [1,*], Ziyang Chen [1], Tushar Sarkar [2], Rakesh Kumar Singh [2] and Jixiong Pu [3,4,*]

[1] College of Information Science and Engineering, Huaqiao University, Xiamen 361021, China; yanyanhuang@stu.hqu.edu.cn (Y.H.); ziyang@hqu.edu.cn (Z.C.)
[2] Laboratory of Information Photonics & Optical Metrology, Department of Physics, Indian Institute of Technology (BHU), Varanasi 221005, Uttar Pradesh, India; tushar.sarkar.rs.phy18@itbhu.ac.in (T.S.); krakeshsingh.phy@iitbhu.ac.in (R.K.S.)
[3] Fujian Provincial Key Laboratory of Light Propagation and Transformation, Huaqiao University, Xiamen 361021, China
[4] Dongguan Guangda Intelligent Technology Co., Ltd., Dongguang, Guangdong 523808, China
* Correspondence: vinurv@hqu.edu.cn (V.R.V.); jixiong@hqu.edu.cn (J.P.)

Abstract: Orbital angular momentum (OAM) of optical vortex beams has been regarded as an independent physical dimension of light with predominant information-carrying potential. However, the presence of scattering environment and turbulent atmosphere scrambles the helical wavefront and destroys the orthogonality of modes in vortex beam propagation. Here, we propose and experimentally demonstrate a new basis for the recovery of the OAM mode using a holographic ghost diffraction scheme. The technique utilizes the speckle field generated from a rotating diffuser for optical vortex mode encoding, and the fourth-order correlation of the speckle field for the efficient recovery of the associated modes. Furthermore, we successfully demonstrate the complex-field recovery of OAM modes by the adoption of a holography scheme in combination with the ghost diffraction system. We evaluate the feasibility of the approach by simulation and followed by experimental demonstration for the recovery of various sequentially encoded OAM modes. Finally, the efficacy of the recovered modes was quantitatively analyzed by an OAM mode analysis utilizing orthogonal projection scheme.

Keywords: holography; ghost diffraction; orbital angular momentum; speckles

Citation: Huang, Y.; R.V., V.; Chen, Z.; Sarkar, T.; Singh, R.K.; Pu, J. Recovery and Characterization of Orbital Angular Momentum Modes with Ghost Diffraction Holography. *Appl. Sci.* **2021**, *11*, 12167. https://doi.org/10.3390/app112412167

Academic Editors: Tomasz Kozacki, David Blinder, Ting-Chung Poon and Andrés Márquez

Received: 3 October 2021
Accepted: 14 December 2021
Published: 20 December 2021

1. Introduction

Optical beams with helical wavefronts and associated orbital angular momentum (OAM) have become a focus of intense research in recent years owing to its high-capacity information bearing characteristics with noteworthy applications in various domains of imaging and communication [1]. The recognition of OAM of helical phase beams by Allen et al. provides new insights into the theoretical and applied realms of optical vortex beams [2]. The vortex-encoded light beams possess an azimuthal phase of $\exp(il\phi)$, where ϕ is the angular coordinate and l is the topological charge that owns a positive or negative sign, and carries an OAM equivalent to $l\hbar$ per photon ($\hbar$ is the Planck's constant divided by 2π) [3]. The orthogonality and infinite-dimensional basis of OAM modes offer extensive applications in OAM multiplexing-based optical communication in free space and optical fiber, quantum and classical information processing, multi-dimensional coding, and imaging [1,4,5]. Following theoretical investigations on the properties of optical vortex beams, several experimental techniques were realized for the generation of helically phased beams by utilizing spiral phase plate (SPP), diffractive optical elements, cylindrical lens with mode converters, q-plates, meta surface, etc. [1]. Recent years have witnessed the extension of the regime of optical vortices from coherent light to low coherent light with the demonstration of helicoidal modes in partially coherent beams [6–8]. The horizon

of partially coherent vortex beams or vortex beams embedded into the randomness has expanded with the demonstration of the existence of phase singularity in the correlation function utilizing the Young-type interference experiment [9], by using broad band light source illumination on a vortex phase mask [10], an irradiance control of an extended quasi monochromatic source [11], with spatial light modulator [12], etc. Moreover, experimental strategies to generate vortices in coherence function by utilizing the partially coherent light arrays were demonstrated by the controlled modulation in the correlation structure of the light fields [13,14].

Along with the advancements in the generation and transmission of optical vortex beams, the detection and sorting of specific OAM modes are an indispensable part in view of the applied domain. A variety of techniques for detection and sorting were demonstrated in the last two decades by utilizing inverse SPPs, holographic gratings, interferometry, mode sorters, etc. [1]. However, the presence of inhomogeneous or turbulent atmosphere inevitably destroys the helical wavefront of the vortex beam, which limits the execution of conventional detection schemes. Last decade saw the introduction of several research efforts that emphasize the development of sophisticated approaches for the recovery and determination of topological charge of vortex beams propagating through rough scattering surface by exploiting the information bearing properties of the speckle pattern generated from the scattering medium [15–19]. In addition, several theoretical investigations on the cross-correlation function of partially coherent optical beams with vortices were demonstrated and techniques were developed for helicity and topological charge determination of partially coherent vortex beams [20–22]. Additionally, the robustness of the low coherent vortex beams in propagation through turbulent and noisy media in comparison to high coherent optical beams was explored [23,24], and a few techniques were demonstrated recently for the discrimination of incoherent vortex states of light [25] and in the sorting of incoherent optical vortex modes [26].

In this article, we propose a speckle correlation assisted quantitative technique for the recovery of OAM modes with a holographic ghost diffraction system. The approach utilizes the robust propagation characteristics of the spatially incoherent light beam comprising the speckle field and exploits the properties of the speckle field to encode and transmit the OAM modes with various topological charges. A spatial light modulator (SLM) is employed for the sequential encoding of various modes, and the information of the OAM modes is recovered from the correlation of spatial intensity fluctuations of the speckle field at the detector plane. Moreover, a simultaneous detection of amplitude and phase of the OAM modes is achieved by adopting the holography scheme by superposing an independent reference random field with the speckle field of the spatially incoherent source. The complex field recovery of OAM modes provides an additional advantage of determining the sign of the topological charge along with the amplitude, which makes the potential realization of the approach in the applied domains of optical storage and communication. Applicability of the proposed technique is theoretically investigated and experimentally demonstrated by recovering the complex correlation functions bearing various OAM modes.

2. Principle and Methods

2.1. Generation and Recovery of OAM Modes

Let us consider a light source created by the coherent light illumination on a rotating ground glass diffuser (RGGD). The speckled beam proceeding from the diffuser illuminates a spatial light modulator (SLM), which encodes the phase mask for vortex beam generation. The beam emanating from the SLM carries the signature of the OAM mode, which is spatially distorted into the random pattern without any direct signature of the mode. A conceptual schematic of the generation of a vortex beam with the proposed technique is illustrated in Figure 1. The speckle field carries the vortex information ($V_0^{\varepsilon l}(\hat{\boldsymbol{r}}) = exp(i\varepsilon l\phi)$) with zero radial index and l azimuthal index, where ε and l represent the sign and magnitude of the topological charge (TC) of the specific OAM mode. The helicity of the specific

mode is determined by ε with $\varepsilon = 1$ for an anticlockwise helical structure direction and $\varepsilon = -1$ for a clockwise direction.

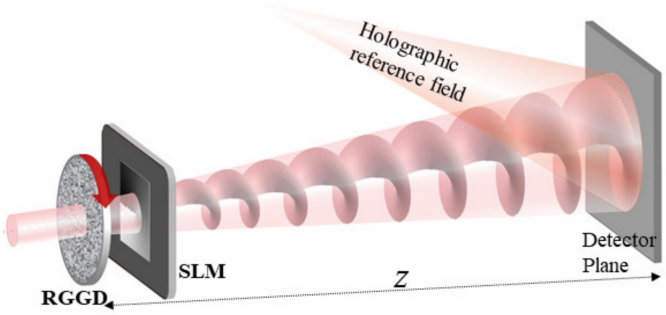

Figure 1. Conceptual schematic of the generation and propagation of a vortex beam with specific OAM mode. The superposition of an independent random reference field with the ghost diffraction fields makes an off-axis ghost diffraction holography scheme; RGGD: rotating ground glass diffuser; SLM: spatial light modulator.

As shown in Figure 1, the speckle field encoded with the specific modes propagates in the positive Z-direction in free space. The field distribution in a transverse plane at distance z from the source plane is given by [27],

$$\psi_l(\boldsymbol{r}) = \frac{\exp(ikz)}{i\lambda z} \int \psi_0(\hat{\boldsymbol{r}}) \exp\left(i\varphi_g(\hat{\boldsymbol{r}})\right) V_0^{\varepsilon l}(\hat{\boldsymbol{r}}) \exp\left[\frac{ik}{2z}\left(|\boldsymbol{r}|^2 - 2\boldsymbol{r}\cdot\hat{\boldsymbol{r}} + |\hat{\boldsymbol{r}}|^2\right)\right] d\hat{\boldsymbol{r}} \quad (1)$$

where $\psi_0(\hat{\boldsymbol{r}})$ is the incident light field at the exit plane of source, $\varphi_g(\hat{\boldsymbol{r}})$ the random phase introduced by the ground glass diffuser, λ the wavelength of the light source, $k = \frac{2\pi}{\lambda}$ the wave number of light, z the propagation distance, and $\hat{\boldsymbol{r}}$ and $\boldsymbol{r}$ are the position coordinates at the source plane and detector plane, respectively. The free space propagating field distribution reaching the detector plane consists of speckle field characterized by Gaussian field statistics [28], where the information of the OAM modes is indistinguishable and scrambled in the random pattern. The cross-correlation of two identical copies of the spatially incoherent field distribution at the detector plane, with one copy $\psi_m(\boldsymbol{r})$ with m having any positive or negative integer values and the other $\psi_0(\boldsymbol{r})$ with a zero-order vortex mode can retain the signature of the OAM modes in its cross-correlation function [29]. Therefore, the cross-correlation of the field contributions $\psi_m(\boldsymbol{r})$ and $\psi_0(\boldsymbol{r})$ is expressed via the field correlation function,

$$W(\boldsymbol{r}_1, \boldsymbol{r}_2) = \langle \psi_m^*(\boldsymbol{r}_1)\psi_0(\boldsymbol{r}_2)\rangle \quad (2)$$

where $\langle\ \rangle$ is the ensemble averaging and $W(\boldsymbol{r}_1, \boldsymbol{r}_2)$ the second order correlation function of the field at the detector plane.

Now, let us turn our attention to the measurement of the field correlation function $W(\boldsymbol{r}_1, \boldsymbol{r}_2)$. By assuming the random field distribution at the detector plane obeys Gaussian statistics, the correlations of the spatial intensity fluctuations or fourth-order field correlation function can be expressed in terms of its second-order correlation function [28,30] as,

$$\langle \Delta I_m(\boldsymbol{r}_1)\Delta I_0(\boldsymbol{r}_2)\rangle = |W(\boldsymbol{r}_1, \boldsymbol{r}_2)|^2 \quad (3)$$

where $I_m(\boldsymbol{r}_1) = \psi_m^*(\boldsymbol{r}_1)\psi_m(\boldsymbol{r}_1)$ and $I_0(\boldsymbol{r}_2) = \psi_0^*(\boldsymbol{r}_2)\psi_0(\boldsymbol{r}_2)$ are the respective intensities at the detector plane, $\Delta I_m(\boldsymbol{r}) = \mathrm{I}_m(\boldsymbol{r}) - I_m(\boldsymbol{r})$. From Equation (3), it is evident that this intensity cross-correlation retrieves only the modulus of $W(\boldsymbol{r}_1, \boldsymbol{r}_2)$; therefore, for the complex correlation function recovery and thereby the simultaneous recovery of amplitude and phase distributions of the OAM mode, we make use of the holography scheme, where a reference random field is combined with the propagated spatially incoherent field as shown in Figure 1. The independent addition of the holographic reference random field [31,32]

$(\psi_R(\boldsymbol{r}))$ with the field contributions $\psi_m(\boldsymbol{r})$ and $\psi_0(\boldsymbol{r})$ modifies the correlation of intensity fluctuations in Equation (3) to:

$$\langle \Delta I_m(\boldsymbol{r}_1) \Delta I_0(\boldsymbol{r}_2) \rangle = \left| W(\boldsymbol{r}_1, \boldsymbol{r}_2) + W^R(\boldsymbol{r}_1, \boldsymbol{r}_2) \right|^2 \tag{4}$$

where $I_m(\boldsymbol{r}_1) = (\psi_m(\boldsymbol{r}_1) + \psi_R(\boldsymbol{r}_1))^* (\psi_m(\boldsymbol{r}_1) + \psi_R(\boldsymbol{r}_1))$ the resultant intensity contribution from $\psi_m(\boldsymbol{r})$ and $\psi_R(\boldsymbol{r})$, $I_0(\boldsymbol{r}_2) = (\psi_0(\boldsymbol{r}_2) + \psi_R(\boldsymbol{r}_2))^* (\psi_0(\boldsymbol{r}_2) + \psi_R(\boldsymbol{r}_2))$ the resultant intensity contribution from $\psi_0(\boldsymbol{r})$ and $\psi_R(\boldsymbol{r})$ with $'\Delta I'$ representing the fluctuation of intensity value with respect to its average value, $W(\boldsymbol{r}_1, \boldsymbol{r}_2) = \psi_m^*(\boldsymbol{r}_1)\psi_0(\boldsymbol{r}_2)$ represents the complex cross-correlation function that bears the OAM mode in its correlation function and $W^R(\boldsymbol{r}_1, \boldsymbol{r}_2) = \psi_R^*(\boldsymbol{r}_1)\psi_R(\boldsymbol{r}_2)$ the reference correlation function. Albeit the execution of ensemble averaging in the approach can be performed either with temporal averaging or with space averaging, we rely on space averaging by considering the time frozen speckle fields at the detector plane under the assumption of spatial stationarity [32–35]. The spatial averaging is performed in the execution of the cross-correlation of intensity images by fixing the distance $\Delta\boldsymbol{r} = \boldsymbol{r}_1 - \boldsymbol{r}_2$ equivalent to the pixel size at the detector plane, and by moving a specific window size in the intensity distribution $I_m(\boldsymbol{r})$ over the entire intensity image $I_0(\boldsymbol{r})$. Equation (4) is the contribution of two complex correlation functions, and thus described as correlation hologram, as in analogous to the conventional holography, but with the superposition of correlation functions [36,37].

Therefore, by considering the change of variables $\boldsymbol{r}_1 = \boldsymbol{r} + \Delta\boldsymbol{r}$ and $\boldsymbol{r}_2 = \boldsymbol{r}$ the complex cross-correlation function $W(\boldsymbol{r}_1, \boldsymbol{r}_2)$ in Equation (4) is expressed by the relation, (see Supplementary Materials)

$$\begin{aligned} \mathrm{W}(\boldsymbol{r} + \Delta\boldsymbol{r}, \boldsymbol{r}) \approx \iint\ & \psi_0^*(\hat{\boldsymbol{r}}_1) V_0^{\varepsilon l}(\hat{\boldsymbol{r}}_1) \psi_0(\hat{\boldsymbol{r}}_2) \delta(\hat{\boldsymbol{r}}_1 - \hat{\boldsymbol{r}}_2) \exp\left[-i\left(\varphi_g(\hat{\boldsymbol{r}}_1) - \varphi_g(\hat{\boldsymbol{r}}_2)\right)\right] \\ & \times \exp\left[-i\tfrac{k}{2z}\left(|\hat{\boldsymbol{r}}_1|^2 - |\hat{\boldsymbol{r}}_2|^2\right)\right] \exp\left[-i\tfrac{2\pi}{\lambda z}\Delta\boldsymbol{r}\cdot\hat{\boldsymbol{r}}_1\right] d\hat{\boldsymbol{r}}_1 d\hat{\boldsymbol{r}}_2 \end{aligned} \tag{5}$$

where $\delta(\hat{\boldsymbol{r}}_1 - \hat{\boldsymbol{r}}_2) \propto \int exp\left[-i\frac{2\pi}{\lambda z}(\hat{\boldsymbol{r}}_1 - \hat{\boldsymbol{r}}_2)\cdot\boldsymbol{r}\right] d\boldsymbol{r}$ the delta function. The contributions of $\boldsymbol{r}$ dependent phase factors $exp\left(ik\frac{|\boldsymbol{r}|^2}{2z}\right)$ and $exp\left(ik\frac{|\boldsymbol{r}+\Delta\boldsymbol{r}|^2}{2z}\right)$ were not represented in Equation (5) as these terms were canceled out while estimating the fourth order correlation using Equation (4). For a fixed wavelength λ and at a fixed propagation distance z, by considering $\hat{\boldsymbol{r}}_2 = \hat{\boldsymbol{r}}_1 = \hat{\boldsymbol{r}}$ the recovered complex cross-correlation function is transformed to,

$$W(\Delta\boldsymbol{r}) \propto \int I_0(\hat{\boldsymbol{r}}) V_0^{\varepsilon l}(\hat{\boldsymbol{r}})\ exp\left[-i\frac{2\pi}{\lambda z}\Delta\boldsymbol{r}\cdot\hat{\boldsymbol{r}}\right] d\hat{\boldsymbol{r}} \tag{6}$$

where $I_0(\hat{\boldsymbol{r}}) = \psi_0^*(\hat{\boldsymbol{r}})\psi_0(\hat{\boldsymbol{r}})$ represents the non-stochastic intensity distribution at the diffuser plane and this appears in Equation (6) without a trace of the random phase $\varphi_g(\hat{\boldsymbol{r}})$. Equation (6) indicates that the correlation function $W(\Delta\boldsymbol{r})$ is directly related to the $I_0(\hat{\boldsymbol{r}})$ and the encoded vortex phase information $V_0^{\varepsilon l}(\hat{\boldsymbol{r}})$ at the exit plane of the diffuser. Additionally, the reference correlation function $W^R(\Delta\boldsymbol{r})$ is considered as, (see Supplementary Materials)

$$W^R(\Delta\boldsymbol{r}) \propto \int I_R(\hat{\boldsymbol{r}})\ exp\left[-i\frac{2\pi}{\lambda z}\Delta\boldsymbol{r}\cdot\hat{\boldsymbol{r}}\right] d\hat{\boldsymbol{r}} \tag{7}$$

where $I_r(\hat{\boldsymbol{r}}) = circ\left(\frac{\hat{\boldsymbol{r}} - \boldsymbol{r}_s}{a}\right)$ is utilized in the proposed approach for the generation of $W^R(\Delta\boldsymbol{r})$ i.e., the intensity of the reference field at off-axis position $'\boldsymbol{r}_s'$ and size $'a'$ of the circular aperture. The reference random field generated by such source creates a constant reference correlation function $W^R(\Delta\boldsymbol{r})$ with a linear phase to record the correlation hologram.

The complex correlation function $W(\Delta\boldsymbol{r})$ is recovered from other redundant terms in Equation (4) by utilizing a Fourier domain filtering approach to the retrieved correlation hologram [38]. Therefore, the recovery of the complex correlation function offers a new method to directly detect OAM modes scrambled in the speckle pattern as explained by

Equation (6). The retrieval of phase distribution along with the amplitude of the vortex modes delivers a direct scheme for the simultaneous determination of sign and magnitude of the topological charge of specific helicity.

2.2. Experimental Design and Recovery Scheme

To demonstrate the applicability of the technique, we develop a vortex beam generation and detection experimental system as shown in Figure 2. The system utilizes the time frozen speckle field detection corresponding to various vortex modes at the detector plane. The experimental technique employs a sequential independent recording of the time frozen speckle fields corresponding to various modes and utilizes the space averaging as a replacement of ensemble averaging in the execution of digital cross-correlation of recorded intensity images. The experimental geometry of the proposed technique is shown in Figure 2a. A spatially filtered and collimated He-Ne laser (632.8 nm) is used as the coherent light source. A non-polarized beam splitter (BS1) splits the beam into two parts, where the transmitted part illuminates a rotating ground glass diffuser (GG1) controlled by an aperture (A) of specific size and generates a spatially incoherent light beam with random speckle field at each instant of time. The instantaneous speckled field from the rotating ground glass illuminates the SLM through a beam splitter (BS2). The reflecting type of phase sensitive SLM (Hamamatsu X131318, 1272 × 1024 pixels, with a pixel pitch of 12.5 μm) is used to encode different vortex modes with specific l values. A half wave plate (HWP) is used to rotate the polarization state of the input beam to match with the polarization sensitivity of the SLM. The reflected beam from BS1 is used to make the holography system by generating an independent reference random field. A point source created by an off-axis microscope objective (MO:10X/0.25NA) illuminates an independent diffuser (GG2) and produces the respective reference random field. This reference random field propagates and combines with the vortex encoded spatially incoherent field by using BS3. The intensity recording is implemented using a charge coupled device (CCD) camera (Prosilica-GT1910 from Allied Vision having total pixels of 1920 × 1080 with a pixel pitch of 5.5 μm, and 57.5 fps). The random light illuminating the SLM further propagates along with the reference random field and is recorded by a CCD, which is synchronized with RGGD and SLM. The vortex phase mask corresponding to various topological charges and zero order phase mask were encoded in the SLM, and the respective time frozen speckle patterns were recorded for various position shifts of the rotating diffuser. The corresponding resultant speckle patterns obtained with specific topological charges are shown in Figure 2b–e. An enlarged view of the marked specific region is shown in the inset of Figure 2b–e, which clearly indicates the speckle pattern modulation with interference fringes corresponding to various vortex phase masks.

A schematic representation of the recovery scheme of OAM modes in the cross-correlation function is shown in Figure 3a. The digital analysis corresponding to vortex phase mask with topological charge $\varepsilon l = +3$ are shown in Figure 3b–i. The phase masks encoded in the SLM are shown in Figure 3b,c. This phase-encoded reflected field individually combined with the reference random field and a double shot recording system records the time frozen intensity images as shown in Figure 3d,e. In the digital processing of two point correlation of intensity fluctuations, spatial averaging is performed by selecting the distance $\Delta \boldsymbol{r}$ with varying the pixel positions $\boldsymbol{r}_1$ and $\boldsymbol{r}_2$ in the double shot recorded intensities $I_m(\boldsymbol{r})$ and $I_0(\boldsymbol{r})$. Therefore, the realization of spatial averaging is carried out by pixel-by-pixel movement of $\Delta I_m(\boldsymbol{r}_1)$ with 200 × 200 pixels over the entire region of $\Delta I_0(\boldsymbol{r}_2)$. This cross-correlation of the intensity fluctuations of the recorded intensities retrieves the correlation hologram as given in Equation (4), which is represented in Figure 3f. The occurrence of a fork type pattern clearly indicates the encoding of the vortex mode in the retrieved correlation hologram. A Fourier domain filtering approach is implemented in the digital processing, where a Fourier transform separates the spectra and its conjugate from the direct carrier (dc) term as shown in Figure 3g. An inverse Fourier transform operation on the filtered and centrally shifted spectrum recovers the cross-correlation function with

the signature of the OAM mode. The recovered amplitude and phase distributions of the OAM mode are shown in Figure 3h,i, respectively.

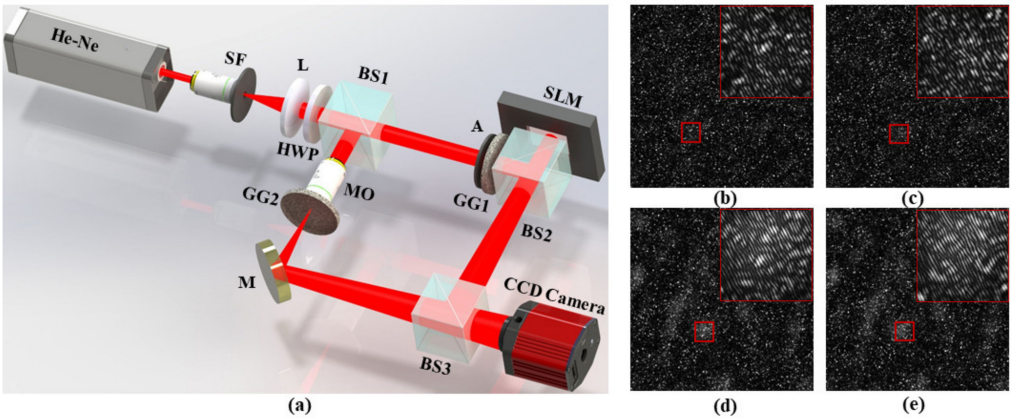

Figure 2. (**a**) Schematic of the experimental system for the generation and recovery of OAM modes: He-Ne, helium-neon laser source; M, mirror; SF, spatial filter assembly; L, lens; HWP, half wave plate; A, aperture; GG, ground glass diffuser; BS, beam splitter; SLM, spatial light modulator; MO, microscope objective; and CCD, charge coupled device camera; (**b**–**e**) CCD recorded resultant speckle pattern for OAM modes with $l = 1,\ 4, -1\ \&\ -4$, respectively.

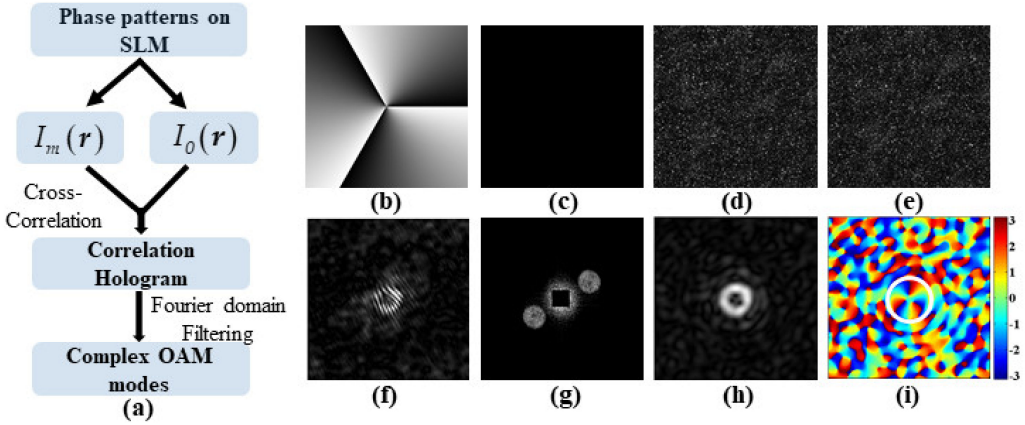

Figure 3. Illustration of the recovery scheme of the technique: (**a**) step by step analysis procedure; (**b**) vortex phase mask ($\varepsilon l = +3$) encoded in the SLM; (**c**) zero order phase mask encoded in the SLM; (**d**,**e**) raw intensity images recorded by the camera corresponding to (**b**,**c**), respectively; (**f**) correlation hologram retrieved from cross-correlation of intensity images; (**g**) results of Fourier transform operation on correlation hologram; (**h**) amplitude distribution of OAM mode; and (**i**) phase distribution of OAM mode.

3. Results and Discussion

3.1. Simulation Results

The proof of principle of the technique is validated by simulation for various vortex modes with specific helicity and topological charge. We simulate the technique by generating a spatially incoherent light source by illuminating a random diffuser with a collimated coherent light source of wavelength 632.8 nm and a beam size of 6.5 mm. Vortex modes of zero radial index with topological charge having $l = 1$ *to* m and $l = 0$ are utilized for generating vortex fields for the correlation function measurement. These fields are holographically added with a random reference field generated from an independent diffuser illuminated with an off-axis point source. The propagated field intensities at the detector plane (with a pixel size of 5.5 μm) at 400 mm from the diffuser plane are considered for performing the cross-correlation of spatial intensity fluctuations. The simulation results corresponding to $\varepsilon l = +1\ \&\ -1$ and $\varepsilon l = +4\ \&\ -4$ are shown in Figure 4. Figure 4a–d

represents the correlation hologram retrieved from the cross-correlation of intensity fluctuations as expressed in Equation (4). The correlation hologram preserves the signature of the vortex mode in the intensity cross-correlation function, which can be clearly seen as the generation of the fork pattern corresponding to different topological values in a way analogous to the fork hologram in conventional off-axis holography. The amplitude and phase distributions of the OAM modes are retrieved from the correlation hologram by utilizing the Fourier domain filtering approach [38], and the corresponding results are shown in Figure 4e–h and Figure 4i–l, respectively.

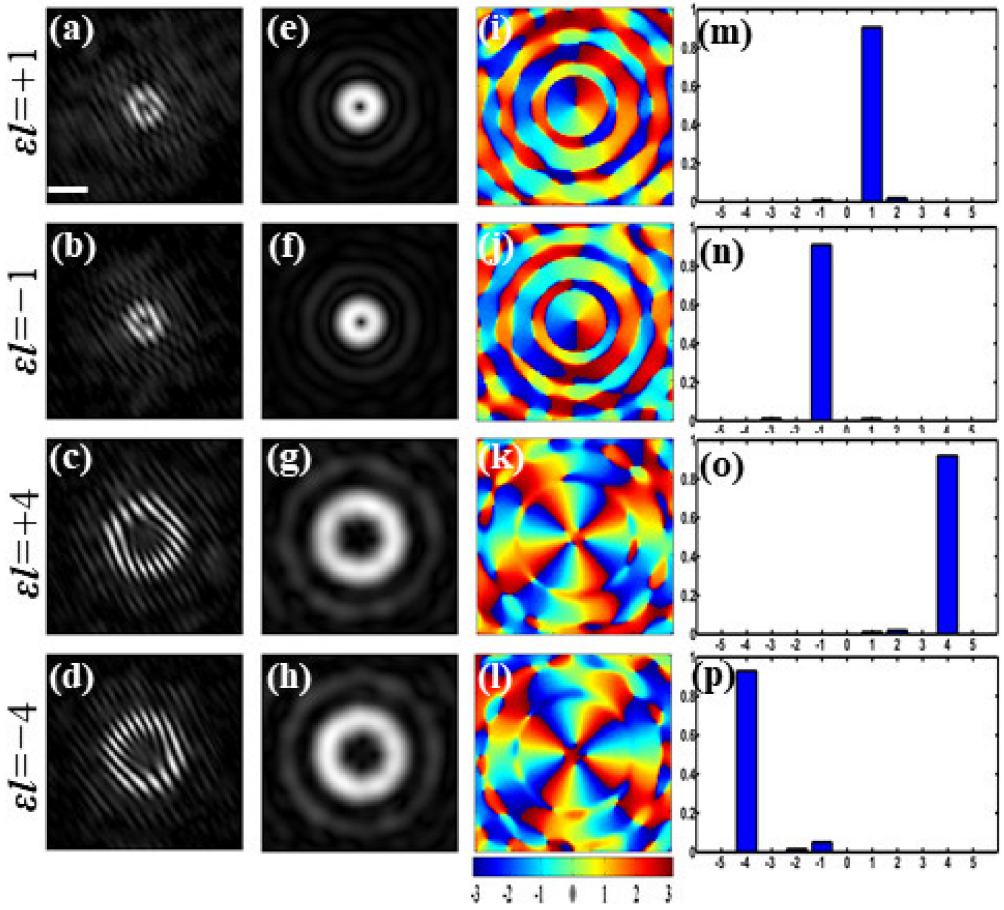

Figure 4. Theoretical simulation results; Simulation results: (**a**–**d**) retrieved correlation holograms; (**e**–**h**) recovered amplitude distributions of the OAM modes; (**i**–**l**) recovered phase distributions of OAM modes; (**m**–**p**) OAM distribution with *X*-axis representing the topological charge (εl) and *Y*-axis the OAM power spectrum ($P(l)$); Scale bar: 110 μm.

3.2. Experimental Results

The sequential encoding of specific phase mask in the SLM generate the vortex beams with various OAM modes. The cross-correlation of CCD recorded intensity fluctuations retrieves the correlation hologram at the detector plane, and the acquired experimental results corresponding to the simulation results (Figure 4) are shown in Figure 5. The SLM is encoded with different vortex phase masks having $\varepsilon l = +1$ & -1, $\varepsilon l = +4$ & -4 and $l = 0$ for generating the respective vortex beams. Figure 5a–d represent the correlation hologram retrieved from the cross-correlation of intensity fluctuations of CCD recorded intensities. The recovered amplitude and phase distributions of the vortex modes for respective topological charges are shown in Figure 5e–h and Figure 5i–l. The amplitude distributions shown in Figure 5e–h show a doughnut shape. The simultaneous recovery of both phase and amplitude provides direct advantage of quantitative determination of magnitude and sign of the topological charge of the generated OAM modes in terms of the recovered phase. The recovered phase distributions shown in Figure 4i–l in simulation and

Figure 5i–l in experiment exhibit a phase variation around the singularity in the order of $2l\pi$ with the number of phase jumps equal to the value of l. Moreover, the quantitative examination of the phase value provides the direct information of the sign of the topological charge from the direction of rotation of the recovered phase distribution of OAM modes. An anticlockwise direction of rotation of phase variation corresponds to the positive and a clockwise direction of rotation corresponds to the negative topological charge.

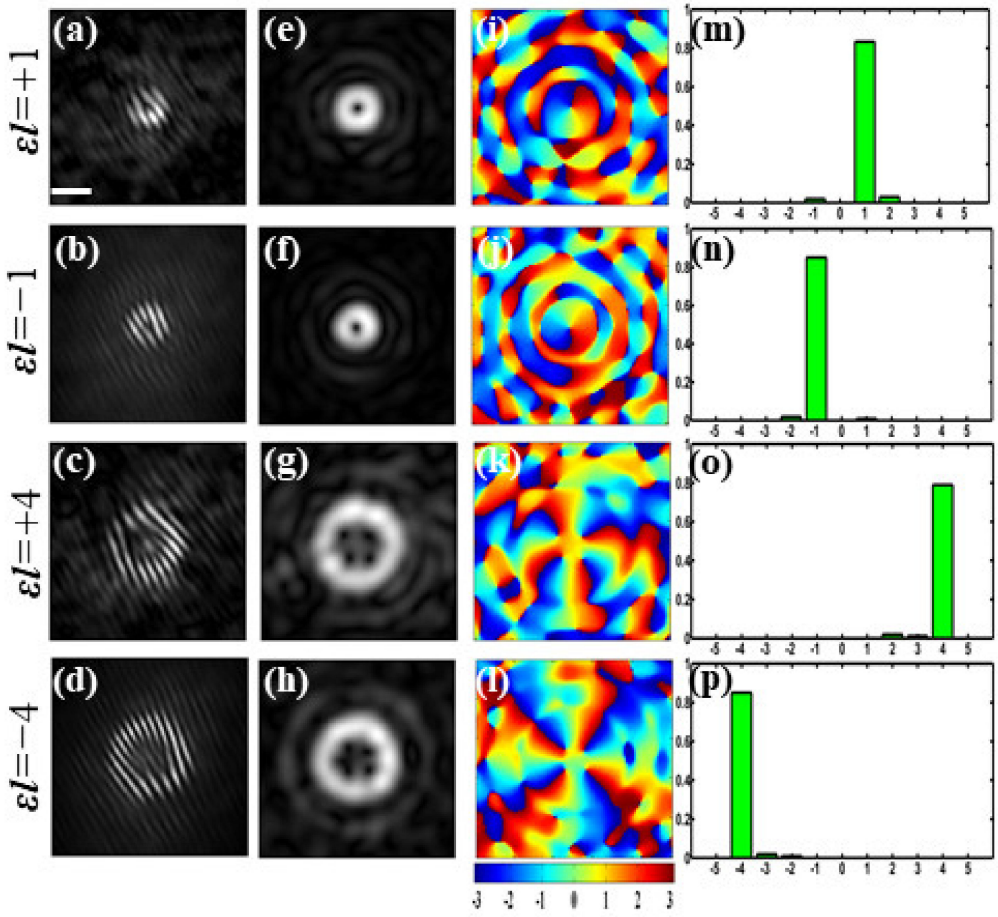

Figure 5. Experimental results: (**a**–**d**) retrieved correlation holograms; (**e**–**h**) recovered amplitude distributions of the OAM modes; (**i**–**l**) recovered phase distributions of the OAM modes; (**m**–**p**) OAM distribution with *X*-axis the topological charge (εl) and *Y*-axis the OAM power spectrum ($P(l)$); Scale bar: 110 μm.

Furthermore, to highlight the applicability of the approach in more applied scenarios, a quantitative analysis of the recovered OAM modes is carried out using orthogonal projection method [19,39]. The OAM power spectrum of recovered modes is determined, and a decomposition is carried out for each OAM component in terms of azimuthal modes. The simulation and experimental results corresponding to the orthogonal projection analysis shown in Figures 4m–p and 5m–p, respectively, exhibits a good agreement. Also, we carry out experimental recovery and characterization of OAM modes with different TCs, and the quantitative characterization results corresponding to $|\varepsilon l| = 1$ *to* 11 are represented in the plot shown in Figure 6. The inner and outer radii of OAM modes were retrieved from the respective amplitude distribution of correlation function [40]. The doughnut structure of the amplitude distribution of OAM mode has a direct dependence with the TC, which is demonstrated in the plot. The plot illustrates the experimentally generated OAM modes of $|\varepsilon l| = 1$ *to* 11 and their corresponding simulation results. Figure 6a represents the variation of inner and outer radii of the recovered modes with various TC. Figure 6b shows the variation of areas of dark core and the annular bright rings of the doughnut structure

with the TC. The quantitative comparison of experimental and theoretical results shows a good agreement for all the recovered modes with various l values. The dark core and the annular bright ring have a direct relation with the order of the OAM mode, where an increase in the order of the vortices makes a corresponding increase in the areas.

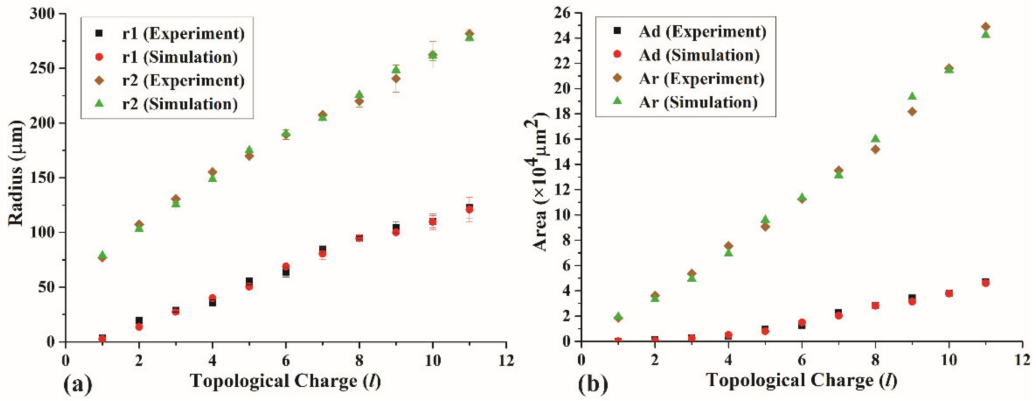

Figure 6. Quantitative comparison of experimental and simulation results: (**a**) variation of inner and outer radii with the topological charge (r_1, inner radius and r_2, outer radius); (**b**) variation of area of dark core (Ad, dark core) and area of bright annular ring (Ar, annular ring) of the recovered OAM modes.

4. Conclusions

In conclusion, we have developed a technique for the recovery and characterization of OAM modes with a ghost diffraction holography system. The approach utilizes the spatial correlation of intensity fluctuations of the speckle pattern for the recovery of scrambled vortex modes. The applicability of the technique is validated by simulation and followed by experimental demonstrations for the recovery of integer orders of various OAM modes with positive or negative helicity. Additionally, we have demonstrated the recovery of phase distribution beside the amplitude distribution of OAM modes and highlighted the advantage of simultaneous determination of sign and magnitude of the topological charge from the direction of rotation and azimuthal order of the helical phase structure. Moreover, the encoding of the OAM modes in random field and the quantitative recovery of scrambled modes from speckle pattern may find significant interest in the sorting of superposed optical vortex modes. In addition, the technique is expected to find important applications in optical communications, multi-dimensional imaging, ghost imaging, coding, imaging through turbid media, etc.

Supplementary Materials: The mathematical derivations are available online at https://www.mdpi.com/article/10.3390/app112412167/s1. References [28,31–34,37] are cited in the supplementary materials.

Author Contributions: Conceptualization, V.R.V.; methodology, Y.H. and V.R.V.; formal analysis, Y.H., T.S., R.K.S. and V.R.V.; investigation, Y.H. and V.R.V.; data curation, Y.H. and V.R.V.; writing—original draft preparation, Y.H. and V.R.V.; writing—review and editing, V.R.V., Z.C., R.K.S. and J.P.; supervision, J.P.; funding acquisition, Z.C. and J.P. All authors have read and agreed to the published version of the manuscript.

Funding: This research was funded by the National Natural Science Foundation of China (NSFC) under grant number 62005086; Dongguan Introduction Program of Leading Innovative and Entrepreneurial Talents under grant number 201927879; Science and Engineering Research Board (SERB) India, grant no. CORE/2019/000026; Council of Scientific and Industrial Research (CSIR), India, grant no. 80 (0092)/20/EMR-II; and the Department of Biotechnology (DBT), India grant no. BT/PR35587/MED/32/707/2019.

Institutional Review Board Statement: Not applicable.

Informed Consent Statement: Not applicable.

Data Availability Statement: The data that support the findings of this study are available from the corresponding author, V.R.V., upon a reasonable request.

Conflicts of Interest: The authors declare no conflict of interest.

References

1. Yao, A.M.; Padgett, M.J. Orbital Angular Momentum: Origins, Behavior and Applications. *Adv. Opt. Photonics* **2011**, *3*, 161. [CrossRef]
2. Allen, L.; Beijersbergen, M.W.; Spreeuw, R.J.C.; Woerdman, J.P. Orbital Angular Momentum of Light and the Transformation of Laguerre-Gaussian Laser Modes. *Phys. Rev. A* **1992**, *45*, 8185–8189. [CrossRef] [PubMed]
3. GBUR, G.J. Singular optics. *Prog. Opt.* **2021**, *42*, 219–276.
4. Chen, R.; Zhou, H.; Moretti, M.; Wang, X.; Li, J. Orbital Angular Momentum Waves: Generation, Detection, and Emerging Applications. *IEEE Commun. Surv. Tutor.* **2020**, *22*, 840–868. [CrossRef]
5. Willner, A.E.; Ren, Y.; Xie, G.; Yan, Y.; Li, L.; Zhao, Z.; Wang, J.; Tur, M.; Molisch, A.F.; Ashrafi, S. Recent Advances in High-Capacity Free-Space Optical and Radio-Frequency Communications Using Orbital Angular Momentum Multiplexing. *Philos. Trans. R. Soc. Math. Phys. Eng. Sci.* **2017**, *375*, 20150439. [CrossRef] [PubMed]
6. Gori, F.; Santarsiero, M.; Borghi, R.; Vicalvi, S. Partially Coherent Sources with Helicoidal Modes. *J. Mod. Opt.* **1998**, *45*, 539–554. [CrossRef]
7. Gbur, G.; Visser, T.D. Phase Singularities and Coherence Vortices in Linear Optical Systems. *Opt. Commun.* **2006**, *259*, 428–435. [CrossRef]
8. Zeng, J.; Lin, R.; Liu, X.; Zhao, C.; Cai, Y. Review on Partially Coherent Vortex Beams. *Front. Optoelectron.* **2019**, *12*, 229–248. [CrossRef]
9. Bogatyryova, G.V.; Fel'de, C.V.; Polyanskii, P.V.; Ponomarenko, S.A.; Soskin, M.S.; Wolf, E. Partially Coherent Vortex Beams with a Separable Phase. *Opt. Lett.* **2003**, *28*, 878. [CrossRef]
10. Palacios, D.M.; Maleev, I.D.; Marathay, A.S.; Swartzlander, G.A. Spatial Correlation Singularity of a Vortex Field. *Phys. Rev. Lett.* **2004**, *92*, 143905. [CrossRef]
11. Wang, W.; Duan, Z.; Hanson, S.G.; Miyamoto, Y.; Takeda, M. Experimental Study of Coherence Vortices: Local Properties of Phase Singularities in a Spatial Coherence Function. *Phys. Rev. Lett.* **2006**, *96*, 073902. [CrossRef]
12. Perez-Garcia, B.; Yepiz, A.; Hernandez-Aranda, R.I.; Forbes, A.; Swartzlander, G.A. Digital Generation of Partially Coherent Vortex Beams. *Opt. Lett.* **2016**, *41*, 3471. [CrossRef]
13. Liu, M.-J.; Chen, J.; Zhang, Y.; Shi, Y.; Zhao, C.-L.; Jin, S.-Z. Generation of Coherence Vortex by Modulating the Correlation Structure of Random Lights. *Photonics Res.* **2019**, *7*, 1485. [CrossRef]
14. Singh, R.K.; Sharma, A.M.; Senthilkumaran, P. Vortex Array Embedded in a Partially Coherent Beam. *Opt. Lett.* **2015**, *40*, 2751. [CrossRef]
15. Jesus-Silva, A.J.; Hickmann, J.M.; Fonseca, E.J.S. Strong Correlations between Incoherent Vortices. *Opt. Express* **2012**, *20*, 19708. [CrossRef]
16. Reddy, S.G.; Prabhakar, S.; Kumar, A.; Banerji, J.; Singh, R.P. Higher Order Optical Vortices and Formation of Speckles. *Opt. Lett.* **2014**, *39*, 4364. [CrossRef]
17. Salla, G.R.; Perumangattu, C.; Prabhakar, S.; Anwar, A.; Singh, R.P. Recovering the Vorticity of a Light Beam after Scattering. *Appl. Phys. Lett.* **2015**, *107*, 021104. [CrossRef]
18. Vinu, R.V.; Singh, R.K. Determining Helicity and Topological Structure of Coherent Vortex Beam from Laser Speckle. *Appl. Phys. Lett.* **2016**, *109*, 111108. [CrossRef]
19. Sarkar, T.; Parvin, R.; Brundavanam, M.M.; Singh, R.K. Higher-Order Stokes-Parameter Correlation to Restore the Twisted Wave Front Propagating through a Scattering Medium. *Phys. Rev. A* **2021**, *104*, 013525. [CrossRef]
20. Yang, Y.; Mazilu, M.; Dholakia, K. Measuring the Orbital Angular Momentum of Partially Coherent Optical Vortices through Singularities in Their Cross-Spectral Density Functions. *Opt. Lett.* **2012**, *37*, 4949. [CrossRef]
21. Ding, P.F.; Pu, J. The Cross Correlation Function of Partially Coherent Vortex Beam. *Opt. Express* **2014**, *22*, 1350. [CrossRef] [PubMed]
22. Lu, X.; Zhao, C.; Shao, Y.; Zeng, J.; Konijnenberg, S.; Zhu, X.; Popov, S.; Urbach, H.P.; Cai, Y. Phase Detection of Coherence Singularities and Determination of the Topological Charge of a Partially Coherent Vortex Beam. *Appl. Phys. Lett.* **2019**, *114*, 201106. [CrossRef]
23. Wang, T.; Pu, J.; Chen, Z. Propagation of Partially Coherent Vortex Beams in a Turbulent Atmosphere. *Opt. Eng.* **2008**, *47*, 036002. [CrossRef]
24. Jesus-Silva, A.J.; Alves, C.R.; Fonseca, E.J.S. Robustness of a Coherence Vortex. *Appl. Opt.* **2016**, *55*, 7544–7549. [CrossRef]
25. Chen, J.; Li, Y. Discrimination of Incoherent Vortex States of Light. *Opt. Lett.* **2018**, *43*, 5595. [CrossRef]
26. Bezerra, D.O.; Amaral, J.P.; Fonseca, E.J.S.; Alves, C.R.; Jesus-Silva, A.J. Sorting of Spatially Incoherent Optical Vortex Modes. *Sci. Rep.* **2020**, *10*, 1–7. [CrossRef]
27. Goodman, J.W. *Introduction to Fourier Optics*; McGraw-Hill: New York, NY, USA, 1996.
28. Goodman, J.W. *Speckle Phenomena in Optics: Theory and Applications*; Roberts & Co.: Sydney, Australia, 2007.
29. Borghi, R.; Gori, F.; Santarsiero, M. Phase and Amplitude Retrieval in Ghost Diffraction from Field-Correlation Measurements. *Phys. Rev. Lett.* **2006**, *96*, 183901. [CrossRef]

30. Reed, I.S. On a Moment Theorem for Complex Gaussian Processes. *IRE Trans. Inf. Theory* **1962**, *8*, 194–195. [CrossRef]
31. Singh, R.K.; Vinu, R.V.; Sharma, M.A. Recovery of Complex Valued Objects from Two-Point Intensity Correlation Measurement. *Appl. Phys. Lett.* **2014**, *104*, 111108. [CrossRef]
32. Vinu, R.V.; Chen, Z.; Singh, R.K.; Pu, J. Ghost Diffraction Holographic Microscopy. *Optica* **2020**, *7*, 1697. [CrossRef]
33. Takeda, M.; Wang, W.; Naik, D.N.; Singh, R.K. Spatial Statistical Optics and Spatial Correlation Holography: A Review. *Opt. Rev.* **2014**, *21*, 849–861. [CrossRef]
34. Takeda, M. Spatial Stationarity of Statistical Optical Fields for Coherence Holography and Photon Correlation Holography. *Opt. Lett.* **2013**, *38*, 3452–3455. [CrossRef]
35. Li, C.; Chen, Z.; Singh, R.K.; Vinu, R.V.; Pu, J. Increasing field of view and signal to noise ratio in the quantitative phase imaging with phase shifting holography based on the Hanbury Brown-Twiss approach. *Opt. Lasers Eng.* **2022**, *148*, 106771. [CrossRef]
36. Kreis, T. *Handbook of Holographic Interferometry*; Wiley-VCH: Weinheim, Germany, 2005; ISBN 3527405461.
37. Singh, R.K.; Vyas, S.; Miyamoto, Y. Lensless Fourier Transform Holography for Coherence Waves. *J. Opt.* **2017**, *19*, 115705. [CrossRef]
38. Takeda, M.; Ina, H.; Kobayashi, S. Fourier-Transform Method of Fringe-Pattern Analysis for Computer-Based Topography and Interferometry. *J. Opt. Soc. Am.* **1982**, *72*, 156–160. [CrossRef]
39. D'Errico, A.; Piccirillo, B.; Cardano, F.; Marrucci, L.; D'Amelio, R. Measuring the Complex Orbital Angular Momentum Spectrum and Spatial Mode Decomposition of Structured Light Beams. *Optica* **2017**, *4*, 1350–1357. [CrossRef]
40. Zhang, J.; Huang, S.-J.; Zhu, F.-Q.; Shao, W.; Chen, M.-S. Dimensional properties of Laguerre-Gaussian vortex beams. *Appl. Opt.* **2017**, *56*, 3556. [CrossRef]